communications earth & environment

Article

A Nature Portfolio journal

https://doi.org/10.1038/s43247-025-02270-9

# Tracking air pollution and $CO_2$ emissions in 13,189 urban areas worldwide using large geospatial datasets



Soo-Yeon Kim [1], Gaige Hunter Kerr [1], Aaron van Donkelaar [2], Randall V. Martin [2], J. Jason West[3] & Susan C. Anenberg [1]

Air pollution and climate change are urgent global concerns, with urban areas contributing heavily to both air pollutants and greenhouse gas emissions. Here we calculate fine particulate matter, nitrogen dioxide, and ozone concentrations and fossil-fuel carbon dioxide emissions per capita in 13,189 urban areas worldwide from 2005 to 2019 and analyze correlations between trends for these pollutants, leveraging recently-developed global datasets. Globally, we found significant increases in ozone (+6%) and small, non-significant changes in fine particulate matter (+0%), nitrogen dioxide (−1%), and fossil-fuel carbon dioxide emissions (+4%). Also, over 50% of urban areas showed positive correlations for all pollutant pairs, though results varied by global region. High-income countries with strong mitigation policies experienced decreases in all pollutants, while regions with rapid economic growth had overall increases. This study shows the impacts of urban environmental initiatives in different regions and provides insights for reducing air pollution and carbon dioxide emissions simultaneously.

With rapid economic and industrial growth across the globe, environmental pollution, including ambient air pollution and greenhouse gases (GHGs), has emerged as one of the most urgent global concerns. Exposure to air pollution is associated with adverse health effects such as morbidity and mortality due to cardiopulmonary diseases and cancer, as well as adverse birth outcomes[1–5]. Ambient particulate matter and ozone were the fourth and 30th leading risk factors for premature deaths worldwide, responsible for ~5.2 million premature deaths in 2021[6], likely a substantial underestimate as only a subset of air pollutants and health endpoints were included. Also, the Intergovernmental Panel on Climate Change Sixth Assessment Report assessed that global surface temperature increased by 1.09 °C (90% uncertainty interval: 0.95–1.20) in 2011–2020 compared to 1850–1900[7]. Climate change has resulted in substantial adverse impacts and irreversible losses to both human health and the environment, for example, through heightened occurrences of extreme weather events, disruption of human systems, diminished water and food security, and declines in biodiversity of ecosystems[7,8].

Urban areas play a pivotal role in emitting air pollutants and GHGs, especially areas experiencing intense urbanization without appropriate emission controls. Urban areas contribute over 70% of global GHG emissions due to dense, anthropogenic pollutant-emitting activities[9]. Similarly, urban areas typically have higher levels of air pollution than non-urban areas, driven by increased polluting sources and their high density[10,11]. Also, urban areas host large populations affected by diseases associated with air pollution. Over half of the global population resides in urban areas, a proportion expected to exceed two-thirds by 2050[12]. Increased air pollution, combined with the larger number of people exposed, results in greater burdens of diseases attributable to air pollution in urban areas[13,14].

Substantial efforts have been undertaken to address environmental challenges globally. For example, the United Nations (UN) established multiple Sustainable Development Goals (SDGs) that focus on creating sustainable cities, expanding clean energy, and fostering climate action[15]. Additionally, the World Health Organization (WHO) has set air quality guidelines (AQGs) for key air pollutants to help countries achieve safe air quality levels and protect public health. On a city level, various mayoral networks, such as the C40 Cities Climate Leadership Group network (C40 Cities) and the International Council for Local Environmental Initiatives–Local Governments for Sustainability, are actively addressing climate change and environmental challenges. C40 Cities, for instance, has launched a Clean Air Accelerator, through which nearly 50 cities have set ambitious air pollutant emission reduction targets and are taking action[16]. Tracking progress towards these goals and guidelines is crucial for

[1]Department of Environmental and Occupational Health, Milken Institute School of Public Health, George Washington University, Washington, DC, USA. [2]Department of Energy, Environmental & Chemical Engineering, Washington University in St. Louis, St. Louis, MO, USA. [3]Department of Environmental Sciences and Engineering, Gillings School of Global Public Health, University of North Carolina, Chapel Hill, NC, USA. e-mail: sanenberg@email.gwu.edu

accurately quantifying disease burdens related to climate change and air pollution, as well as assessing the societal benefits of actions taken to achieve progress.

Recent advances in satellite remote sensing and geospatial modeling methods have led to improvements in global gridded pollution datasets, which allow for more accurate and consistent estimation of urban air pollution and GHG emissions worldwide[13,17–21]. For example, in 2022, three studies estimated air pollutant concentrations and associated disease burdens in ~13,000 cities globally, each for one of three ubiquitous air pollutants: fine particulate matter with an aerodynamic diameter ≤2.5 μm ($PM_{2.5}$), nitrogen dioxide ($NO_2$), and ozone ($O_3$)[13,20,21]. While these studies provided comprehensive urban estimates for each pollutant individually, exploring relationships between temporal trends among these pollutants and fossil-fuel carbon dioxide ($FFCO_2$) emissions can reveal additional insights. Because air pollutants and GHGs are largely co-emitted from fossil fuel and biofuel combustion[22], positive or negative correlations among air pollutants and GHGs, hereafter collectively referred to as "pollutants", can suggest drivers of these trends. For example, rising $FFCO_2$ coupled with declining $NO_2$ might indicate that end-of-pipe emission controls are reducing $NO_2$ while carbon-based fuel combustion is continuing to emit $FFCO_2$ unabated[22]. Declining $FFCO_2$ and $NO_2$ might indicate that fossil fuel combustion itself is declining—either through population decreases, increased energy efficiency, or transitions to renewable energy and electrification[22]. Conversely, increasing $FFCO_2$ and $NO_2$ simultaneously could indicate that emission sources are growing. Also, trends in these pollutants are influenced to varying degrees by natural sources (e.g., wildland fires, windblown dust), which are also increasingly linked to climate change and human activities in the long term[23]. However, most studies investigating relationships among these pollutants are based on emission scenarios rather than historical observations[24–26], limiting our ability to analyze these relationships in real-world conditions.

This study aims to develop a multi-pollutant database for all urban areas worldwide and to analyze temporal trends of the four pollutants during 2005–2019, where datasets for each pollutant are available and were not influenced by the COVID-19 pandemic. We firstly calculate population-weighted average concentrations of $PM_{2.5}$, $NO_2$, and $O_3$, as well as $FFCO_2$ emissions per capita across 13,189 urban areas, leveraging recently-developed global gridded datasets of these pollutants and applying consistent methods to enable inter-city comparisons, and then test the correlations between temporal trends of these pollutants. Additionally, since governmental and non-governmental actors use different approaches for defining urban areas, we explore the influence of urban boundary definitions on urban pollution estimates and their temporal trends.

## Results

### Global distributions in 2019

In 2019, the global mean of population-weighted annual average $PM_{2.5}$ concentrations across all urban areas was 37.7 μg/m$^3$, which was 7.5 times larger than the WHO AQG of 5 μg/m$^3$ (Fig. 1). The global mean of urban $NO_2$ concentrations was 7.1 ppb, exceeding the WHO AQG (5.3 ppb ≈ 10 μg/m$^3$) by 34%. The global mean of urban $O_3$ concentrations (ozone season daily maximum 8 h mixing ratios (OSDMA8), see details in Methods) was 51.2 ppb, which was 67% higher than the WHO AQG (30.6 ppb ≈ 60 μg/m$^3$). The global median of $FFCO_2$ per capita across all urban areas was 2.8 metric tons in 2019.

We found distinct geographical patterns between urban $PM_{2.5}$, $NO_2$, and $O_3$ concentrations and $FFCO_2$ per capita in 2019; nevertheless, some similar patterns emerged across pollutants with certain regions consistently standing out as hotspots (Fig. 1). Among all the cities, the highest levels of $PM_{2.5}$ were primarily observed in India (Indian cities mean: 61.5 vs. global mean: 37.7 μg/m$^3$), forming a highly polluted cluster in South Asia alongside cities in Bangladesh and Pakistan. Also, we observed clusters of urban areas with high $PM_{2.5}$ levels (> 90th percentile across all urban areas globally; 72.2 μg/m$^3$) in Nigeria, Saudi Arabia, and China. Urban areas with elevated $NO_2$ levels, exceeding the 90th percentile (12.1 ppb), were primarily in China and High-income countries (based on the Global Burden of Disease (GBD) super-region categorization, see details in Supplementary Fig. 1 and Methods). For $O_3$, similarly to $PM_{2.5}$, cities in India had the highest levels, averaging 66.7 ppb which is 30% greater than the global mean (51.2 ppb). Urban areas in only five countries–India, Pakistan, Nepal, China, and Bangladesh–were observed to surpass the 90th percentile of $O_3$ concentrations (69.3 ppb), forming a highly-polluted cluster in South Asia and Southeast Asia, East Asian, and Oceania super-regions. Lastly, urban areas with $FFCO_2$ per capita levels greater than 90th percentile (19.0 metric tons) were heterogeneously distributed worldwide. The majority of cities above the 90th percentile were in China (25%), India (18%), and Iran (5%). When we compared spatial patterns across the pollutants, we found overall consistent geographical distributions of highly polluted cities, particularly between $PM_{2.5}$ and $O_3$ concentrations. South Asia (largely due to India) and China commonly had relatively higher levels of $PM_{2.5}$ and $O_3$ concentrations compared to other regions. Accordingly, in additional analysis, $PM_{2.5}$ and $O_3$ showed the strongest positive correlation ($r = 0.69$ and $p$-value < 0.0001) among all the possible pairs of pollutants in 2019 (Supplementary Fig. 2). When testing correlations separately in each GBD super-region, while this analysis showed different results of correlations across GBD super-regions, all GBD super-regions showed positive correlations with statistical significance between $PM_{2.5}$ and $O_3$, except for Latin America and Caribbean (Supplementary Fig. 2).

### Temporal trends for 2005–2019

We also found different temporal trends across population-weighted annual average $PM_{2.5}$, $NO_2$, and OSDMA8 ($O_3$) concentrations and $FFCO_2$ per capita (Fig. 2). Globally, urban $PM_{2.5}$ concentrations showed an increase from 37.2 μg/m$^3$ in 2005 to a peak of 41.4 μg/m$^3$ in 2011, followed by a decline to 37.7 μg/m$^3$ in 2019. Across GBD super-regions, South Asia showed the highest $PM_{2.5}$ levels throughout the entire study period and even the largest increase from 51.5 μg/m$^3$ in 2005 to 61.4 μg/m$^3$ in 2019. Central Europe, Eastern Europe, and Central Asia; Latin America and Caribbean; and High-income countries exhibited lower $PM_{2.5}$ concentrations than the global mean over the entire study period with constant or decreasing trends. The global mean of urban $NO_2$ concentrations showed little change across the study period, remaining within the range of 7.0−7.4 ppb. High-income countries; Southeast Asia, East Asia, and Oceania; and Central Europe, Eastern Europe, and Central Asia showed higher $NO_2$ levels than the global mean. However, $NO_2$ concentrations had steadily decreased in High-income countries and Central Europe, Eastern Europe, and Central Asia. The global mean of urban $O_3$ concentrations increased from 46.9 ppb in 2005 to 51.2 ppb in 2019. South Asia and Sub-Saharan Africa showed the greatest increases (54.6–66.3 ppb in South Asia and 40.1 to 46.2 ppb in Sub-Saharan Africa). Notably, South Asia maintained the highest $O_3$ concentrations among all the regions. The global median of urban $FFCO_2$ per capita did not show large fluctuations from 2005 (2.56 metric tons) to 2019 (2.77 metric tons). High-income countries; Central Europe, Eastern Europe, and Central Asia; and North Africa and Middle East exhibited the highest levels of $FFCO_2$ per capita over the study period. Among these regions, only High-income countries showed a consistent decrease from 6.23 metric tons in 2005 to 5.12 metric tons in 2019. Temporal trends in North Africa and Middle East experienced increases in $FFCO_2$ per capita until 2011 to decreasing trends afterward, resulting in an overall decline over the whole study period (2005: 4.60 metric tons, 2011: 5.06 metric tons, and 2019: 3.88 metric tons). In contrast, Central Europe, Eastern Europe, and Central Asia showed decreasing trends until 2014 to increasing trends afterward, which led to a small overall decrease (2005: 5.26 metric tons, 2014: 4.43 metric tons, and 2019: 5.09 metric tons). Southeast Asia, East Asia, and Oceania experienced a consistent increase from 2.61 metric tons in 2005 to 3.24 metric tons in 2019, starting to exceed the global median in 2010.

When considering the temporal trends of the four pollutants simultaneously as percent changes from the average values from 2005−2007 to

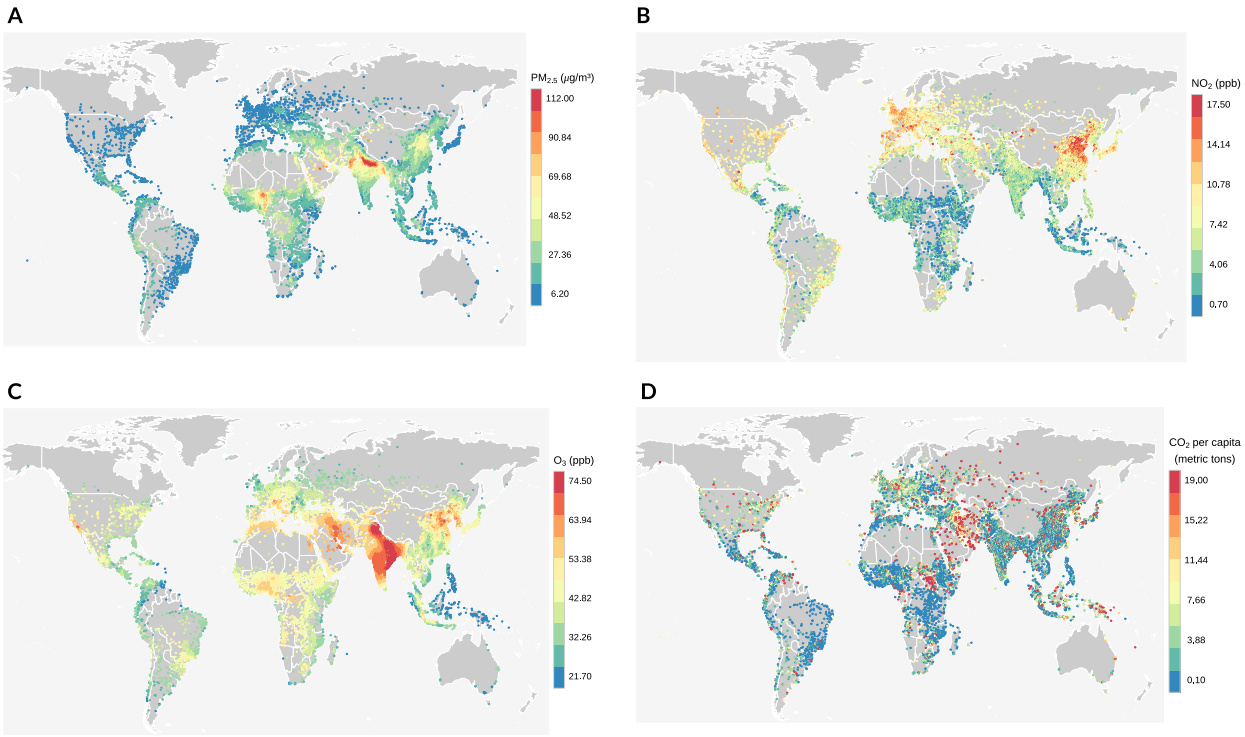


**Fig. 1 | Global distributions of population-weighted annual average $PM_{2.5}$, $NO_2$, and OSDMA8 ($O_3$) concentrations, and $FFCO_2$ per capita in urban areas in 2019.** Values under the 1st percentile or above the 99th percentile (90th percentile for $FFCO_2$ per capita) were consolidated as 1st percentile or 99th/90th percentile values. **A** Population-weighted annual average $PM_{2.5}$ (μg/m$^3$), where $n$ = 13,186, mean = 37.7 μg/m$^3$, 1st percentile = 6.2 μg/m$^3$, and 99th percentile = 112.0 μg/m$^3$. **B** Population-weighted annual average $NO_2$ (ppb), where $n$ = 13,036, mean = 7.1 ppb, 1st percentile = 0.7 ppb, and 99th percentile = 17.5 ppb. **C** Population-weighted OSDMA8 ($O_3$) (ppb), where $n$ = 12,942, mean = 51.2 ppb, 1st percentile = 21.7 ppb, and 99th percentile = 74.5 ppb. **D** $FFCO_2$ per capita (metric tons), where $n$ = 13,185, median = 2.8 metric tons, 1st percentile = 0.1 metric tons, and 90th percentile = 19.0 metric tons. Dark gray areas indicate lands, light gray areas indicate oceans, and white lines indicate country boundaries.

those from 2017–2019, we found unique patterns varying by GBD super-region (Fig. 3). Regarding global trends, only urban $O_3$ concentration showed a statistically significant trend, an increase of 6%. Global urban $PM_{2.5}$, $NO_2$, and $FFCO_2$ per capita in 2017–2019 remained at levels similar to those in 2005–2007 ($PM_{2.5}$: +0%, $NO_2$: −1%, and $FFCO_2$ per capita: +4%), and these trends were not statistically significant. Across all the regions, only High-income countries showed declining trends in all four pollutants with statistical significance ($PM_{2.5}$: −19%, $NO_2$: −7%, $O_3$: −4%, and $FFCO_2$ per capita: −17%). Central Europe, Eastern Europe, and Central Asia showed significantly decreasing trends in three air pollutants ($PM_{2.5}$: −9%, $NO_2$: −5%, and $O_3$: −7%) but not in $FFCO_2$ per capita. In contrast, no decreasing trends were observed in Latin America and Caribbean; South Asia; and Sub-Saharan Africa. Latin America and Caribbean had non-significant/unchanging trends except for $O_3$ (+ 5%). South Asia showed the greatest increases with statistical significance in $PM_{2.5}$ (+14%) and $O_3$ (+18%) among all the regions. Sub-Saharan Africa showed simultaneous increases in $NO_2$ (+9%), $O_3$ (+9%), and $FFCO_2$ per capita (+8%). Regions with slowed population growth during the study period (Central Europe, Eastern Europe, and Central Asia and High-income countries) had overall decreasing trends, in contrast to regions with high-growing populations such as Latin America and Caribbean; South Asia; and Sub-Saharan Africa (Fig. 3).

The other two regions–North Africa and Middle East and Southeast Asia, East Asia, and Oceania–showed opposing trends between air pollutants and $FFCO_2$ per capita. North Africa and Middle East experienced increasing trends in air pollutants ($NO_2$: +3% and $O_3$: +5%) but a decreasing trend in $FFCO_2$ per capita (−14%), while Southeast Asia, East Asia, and Oceania showed the opposite pattern of decreasing air pollution ($PM_{2.5}$: −20% and $O_3$: −6%) and increasing $FFCO_2$ per capita (+22%). The observed trends in Southeast Asia, East Asia, and Oceania were largely driven by urban areas in China, which constituted 63% of the urban areas in the GBD super-region. Additionally, in the top 20 most populous global cities, Osaka/Kyoto was the only city exhibiting significant decreases in all four pollutants (Supplementary Fig. 3). None of these cities met the WHO AQGs for $PM_{2.5}$ and $NO_2$, and most cities except for Quezon City/Manila did not meet $O_3$ WHO AQG in 2019.

For all six pairwise combinations between the four pollutants, over 50% of urban areas had positive correlations (including both significant and non-significant correlations) between pollutant trends globally ($PM_{2.5}$-$NO_2$: 62%, $PM_{2.5}$-$O_3$: 68%, $PM_{2.5}$-$FFCO_2$ per capita: 58%, $NO_2$-$O_3$: 57%, $NO_2$-$FFCO_2$ per capita: 57%, and $O_3$-$FFCO_2$ per capita: 54%, Fig. 4). Over 20% of urban areas had a significant positive correlation ($PM_{2.5}$-$NO_2$: 21%, $PM_{2.5}$-$O_3$: 26%, $PM_{2.5}$-$FFCO_2$ per capita: 20%, $NO_2$-$O_3$: 20%, $NO_2$-$FFCO_2$ per capita: 24%, and $O_3$-$FFCO_2$ per capita: 24%). The highest percentages of positive correlations for $PM_{2.5}$-$O_3$ among these pairs were consistent with the findings from the cross-sectional comparison in 2019. When cities were divided into relatively larger versus smaller cities based on population size, using a population threshold of 50,000, the large city group (51% of all urban areas) had a greater proportion of significant positive correlations for every pair compared to all cities combined ($PM_{2.5}$-$NO_2$: 33%, $PM_{2.5}$-$O_3$: 29%, $PM_{2.5}$-$FFCO_2$ per capita: 28%, $NO_2$-$O_3$: 22%, $NO_2$-$FFCO_2$ per capita: 29%, and $O_3$-$FFCO_2$ per capita: 26%, Supplementary Fig. 4B). In contrast, the small city group (49% of all urban areas) showed a lower proportion of significant positive correlations ($PM_{2.5}$-$NO_2$: 9%, $PM_{2.5}$-$O_3$: 24%, $PM_{2.5}$-$FFCO_2$ per capita: 12%, $NO_2$-$O_3$: 18%, $NO_2$-$FFCO_2$ per capita: 19%, and $O_3$-$FFCO_2$ per capita: 21%, Supplementary Fig. 4A).

The GBD super-regions exhibited different correlation patterns (Fig. 4), which generally aligned with the patterns of temporal trends in

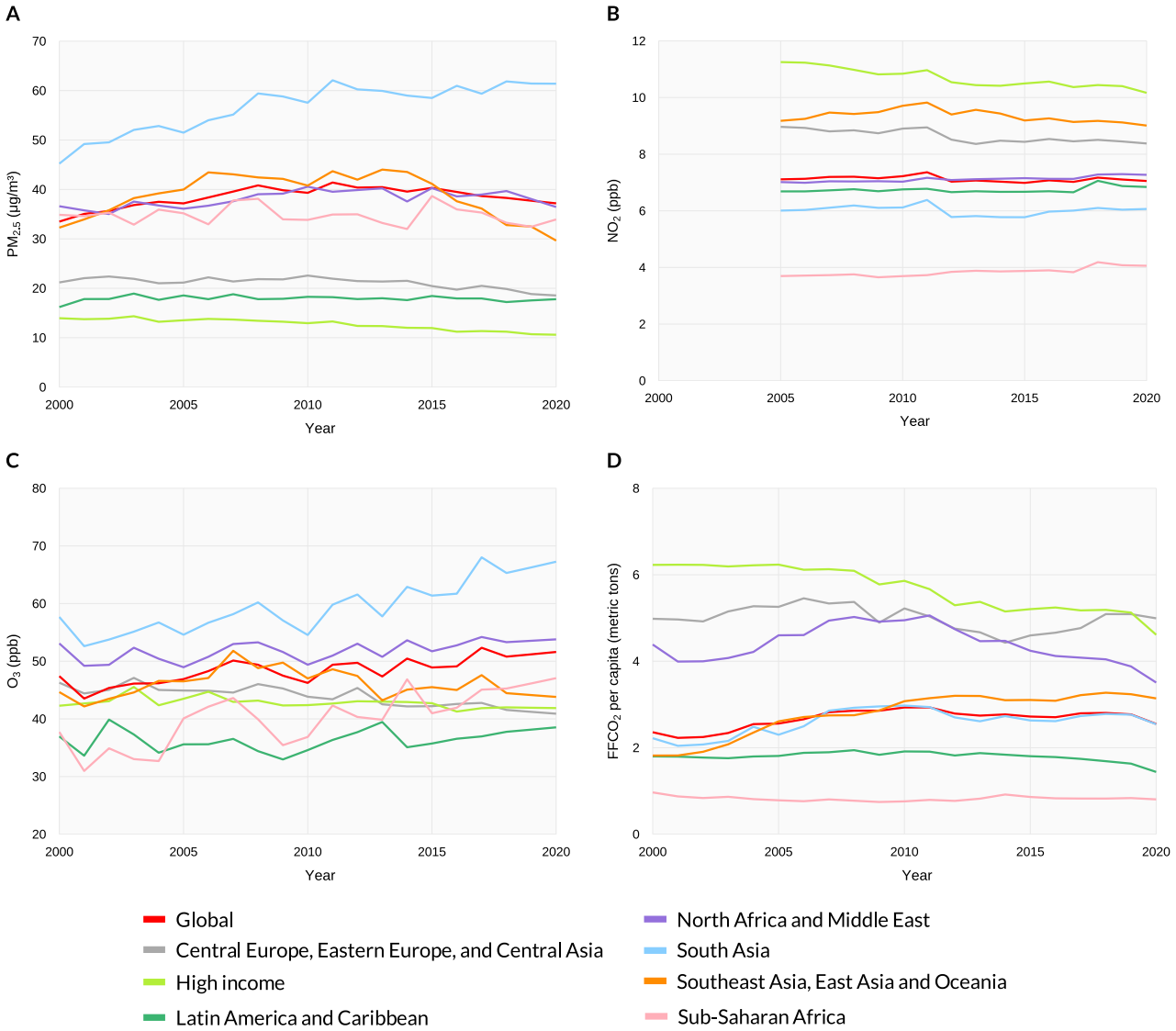


**Fig. 2 | Time-series of population-weighted annual average $PM_{2.5}$, $NO_2$, and OSDMA8 ($O_3$) concentrations, and $FFCO_2$ per capita.** **A** Population-weighted annual average $PM_{2.5}$ (μg/m$^3$, regional mean); $n$ = 13,185. **B** Population-weighted annual average $NO_2$ (ppb, regional mean); $n$ = 12,981. **C** Population-weighted OSDMA8 ($O_3$) (ppb, regional mean); $n$ = 12,941. **D** $FFCO_2$ per capita (metric tons, regional median); $n$ = 13,182. Only urban areas with full-time series available between 2000 (2005 for $NO_2$) and 2019 for each pollutant were included.

Fig. 3. In Central Europe, Eastern Europe, and Central Asia and High-income countries, where overall simultaneous decreases were observed, over 20% of urban areas showed a significant positive correlation for every pair, resulting in high percentages of total positive correlations (including both significant and non-significant positive correlations) ranging from 53% to 92%. South Asia also showed relatively high percentages of urban areas with total positive correlations over 43%. We observed cases that urban areas with negative correlations are more or equally prominent as those with positive correlations, particularly in Latin America and Caribbean and North Africa and Middle East (total positive correlations ranging from 38 to 61%), where coupling trends were rarely found between pollutants in Fig. 3. Southeast Asia, East Asia, and Oceania and Sub-Saharan Africa had mixed patterns depending on pollutants. As Southeast Asia, East Asia, and Oceania showed opposing or decoupling trends between air pollution and $FFCO_2$ per capita, pairs that included $FFCO_2$ per capita had higher percentages of total negative correlations than the other pairs (49–61% for pairs with $FFCO_2$ per capita vs. 20–43% otherwise). In Sub-Saharan Africa, we found higher percentages of total negative correlations for pairs with $PM_{2.5}$ (56–66% for pairs with $PM_{2.5}$ vs. 25–45% otherwise), which was the only pollutant not exhibiting coupling trends with the other pollutants in Fig. 3.

## Urban boundary analysis

We next compared urban $PM_{2.5}$, $NO_2$, and $O_3$ concentrations and $FFCO_2$ per capita using two different urban boundaries: built-up area from the Global Human Settlement Model grid (GHS-SMOD) dataset and administrative boundaries using the C40 Cities dataset (urban boundaries comparison in Supplementary Fig. 5). In 92 urban areas present in both datasets (90 urban areas for $O_3$ due to missing values in the $O_3$ dataset), $PM_{2.5}$ and $O_3$ concentrations showed high agreement between estimates from the two urban boundary definitions, with correlation coefficients ($r$) near 1.00 and $p$-values < 0.0001 (Figs. 5 and 6). $NO_2$ showed lower agreement when compared to $PM_{2.5}$ and $O_3$, but still high agreement of $r$ = 0.78 ($p$-value < 0.0001) in 2019 concentration estimates, as well as high agreement in temporal trends for 2005-2019 ($r$ = 0.99 and $p$-value < 0.0001). We found moderate correlations for $FFCO_2$ per capita across the two urban boundary definitions in both annual concentration estimates in 2019 ($r$ = 0.67 and p-value < 0.0001) and temporal trends for 2005–2019 ($r$ = 0.49 and $p$-value < 0.0001). However, the correlation for temporal trends improved when excluding an extreme point having over +300% change from the C40 Cities definition (Fig. 6), resulting in stronger correlation ($r$ = 0.75 and $p$-value < 0.0001). The C40 Cities definition resulted in higher $FFCO_2$ per capita than the GHS-

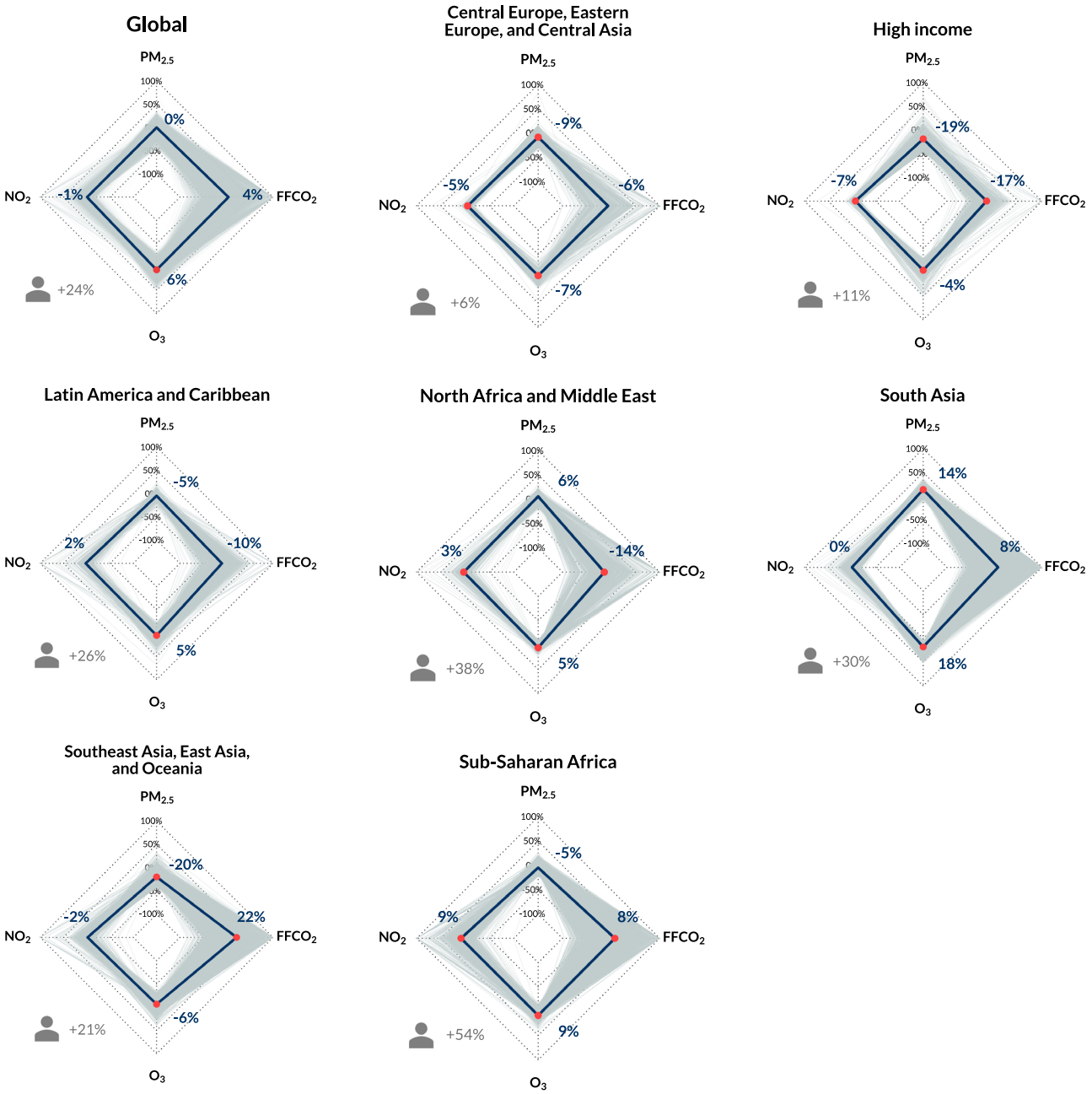


**Fig. 3 | Percent changes in population-weighted annual average $PM_{2.5}$, $NO_2$, and OSDMA8 ($O_3$) concentrations and $FFCO_2$ per capita in urban areas from 2005–2007 to 2017–2019.** Gray lines indicate percent changes in individual cities located within each region, and navy lines indicate percent changes of averaged values across all cities in each region. Red dots indicate statistically significant monotonic trends between 2005 and 2019. Person icons indicate percent changes in total population from 2005−2007 to 2017–2019. Values above 100% were consolidated as 100%. Only urban areas with full-time series available between 2005 and 2019 for every pollutant were included. Global: $n$ = 12,730; Central Europe, Eastern Europe, and Central Asia: $n$ = 605; High income: $n$ = 1243; Latin America and Caribbean: $n$ = 885; North Africa and Middle East: $n$ = 1185; South Asia: $n$ = 3858; Southeast Asia, East Asia, and Oceania: $n$ = 2789; and Sub-Saharan Africa: $n$ = 2165.

SMOD (mean: 3.48 vs 4.49 metric tons and median: 2.19 vs 2.37 metric tons, respectively; Supplementary Table 1).

Differences in estimates of three criteria air pollutants using the two urban definitions did not lead to large differences in the numbers of cities exceeding the WHO interim targets and AQGs (Supplementary Table 2). However, different definitions resulted in different numbers of urban population living in cities exceeding the WHO interim targets and AQGs, even when cities exceeding a guideline were the same. This discrepancy arose because the total population of each city was estimated differently from the two urban boundaries. For example, although all 92 cities exceeded $PM_{2.5}$ AQG, urban population in these cities was estimated as 771 million people from the GHS-SMOD definition and 548 million people from the C40 Cities definition. Differences in pollutant levels between the two urban definitions in 2019 were correlated with several urban characteristics, including total area, differences in total area, and differences in total population (Supplementary Table 3 and Supplementary Fig. 6). For instance, using an urban definition with a larger total area would likely result in lower urban $NO_2$ concentrations and higher $O_3$ concentrations and $FFCO_2$ per capita.

## Discussion

We developed a globally consistent, multi-pollutant database of population-weighted annual average $PM_{2.5}$, $NO_2$, and OSDMA8 ($O_3$)

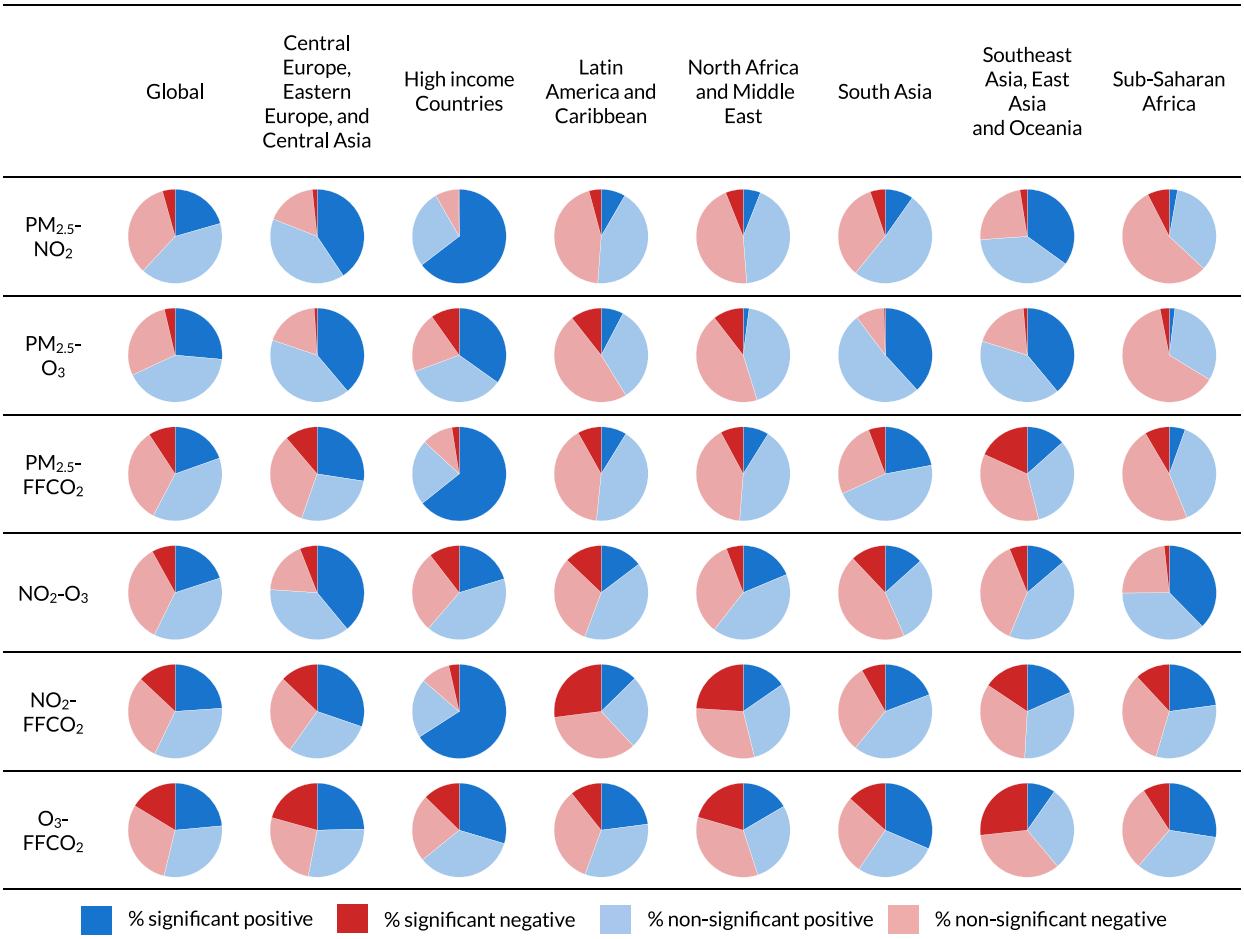


**Fig. 4 | Percent of cities with each type of correlation between pollutant trends.** Only urban areas with full time series available between 2005 and 2019 for every pollutant were included. Global: $n = 12{,}730$; Central Europe, Eastern Europe, and Central Asia: $n = 605$; High income: $n = 1243$; Latin America and Caribbean: $n = 885$; North Africa and Middle East: $n = 1185$; South Asia: $n = 3858$; Southeast Asia, East Asia, and Oceania: $n = 2789$; and Sub-Saharan Africa: $n = 2165$.

concentrations and $FFCO_2$ emissions for all urban areas worldwide, which can be utilized for tracking the progress of urban areas toward achieving WHO guidelines and SDGs. Across these urban areas, we found a significant 6% increase in $O_3$ concentrations globally from 2005–2007 to 2017–2019 and relatively small or no changes in $PM_{2.5}$, $NO_2$, and $FFCO_2$ per capita (+0%, −1%, and +4%, respectively). Across a majority of the global urban areas considered in our study, the four pollutants were positively correlated with one another, reflecting that these pollutants and/or their precursors tend to be co-emitted and have the potential to be reduced simultaneously through mitigation. However, there were substantial variations in temporal trends and correlations by GBD super-region. For example, High-income countries showed significant decreasing trends in all four pollutants and predominantly showed positive correlations across all pollutant pairs. Contrastingly, South Asia and Sub-Saharan Africa showed large significant increases in air pollution and/or $FFCO_2$ per capita during the study period, resulting in high percentages of positive correlations among trends of certain pollutant pairs. In Latin America and Caribbean and North Africa and Middle East, which exhibited decoupling or opposing trends between pollutants, there were similar or even higher numbers of urban areas with negative correlations compared to those with positive correlations.

This study updates urban estimates of air pollution and $CO_2$ emissions from previous literature by using newer global gridded datasets and reaches broadly consistent conclusions as previous studies. A previous study reported similar $PM_{2.5}$ trends in urban areas globally, characterized by an initial increase between 2000-2011 followed by a decline[21]. Also, some studies reported a similar spatial distribution of urban $PM_{2.5}$ concentrations in recent years (2019–2020) across global regions, for example, the highest $PM_{2.5}$ concentrations observed in South Asia[21,27]. We also observed consistent global and region-specific increases (rapid increases in South Asia and Sub-Saharan Africa) in urban $O_3$ concentrations with previous studies that used similar datasets and methodologies as this study[13,18]. For $FFCO_2$ per capita, although direct comparisons with previous studies were not possible due to variations in data sources and spatial units of estimation (e.g., cities, states, and countries), we found consistent temporal trends with previous studies. Increasing $FFCO_2$ per capita in Southeast Asia, East Asia, and Oceania and Sub-Saharan Africa as well as decreasing trends in High-income countries observed in this study were consistently found in previous studies[28–31].

However, urban $NO_2$ trends were inconsistent with previous literature. Globally, we found a 1% non-significant decrease between 2005–2007 and 2017–2019, while Anenberg et al. found a 13% decrease between 2000 and 2019, resulting from a rapid decline after 2010[20]. This difference might stem from different predictors and statistical methods used by the land-use regression (LUR) models, and ground-level monitoring data used for training the LUR models. We used a recently-developed $NO_2$ datasets from Larkin et al., which predicted surface $NO_2$ concentrations at 50 m resolution with Ozone Monitoring Instrument (OMI) column $NO_2$ and twenty land-use and meteorological variables, trained by 8250 monitors globally[32], while Anenberg et al. predicted $NO_2$ concentrations at 1 km resolution with OMI column $NO_2$ and ten land-use and meteorological variables, trained by ground-level $NO_2$ data from 5220 monitors[20]. Also, when computing

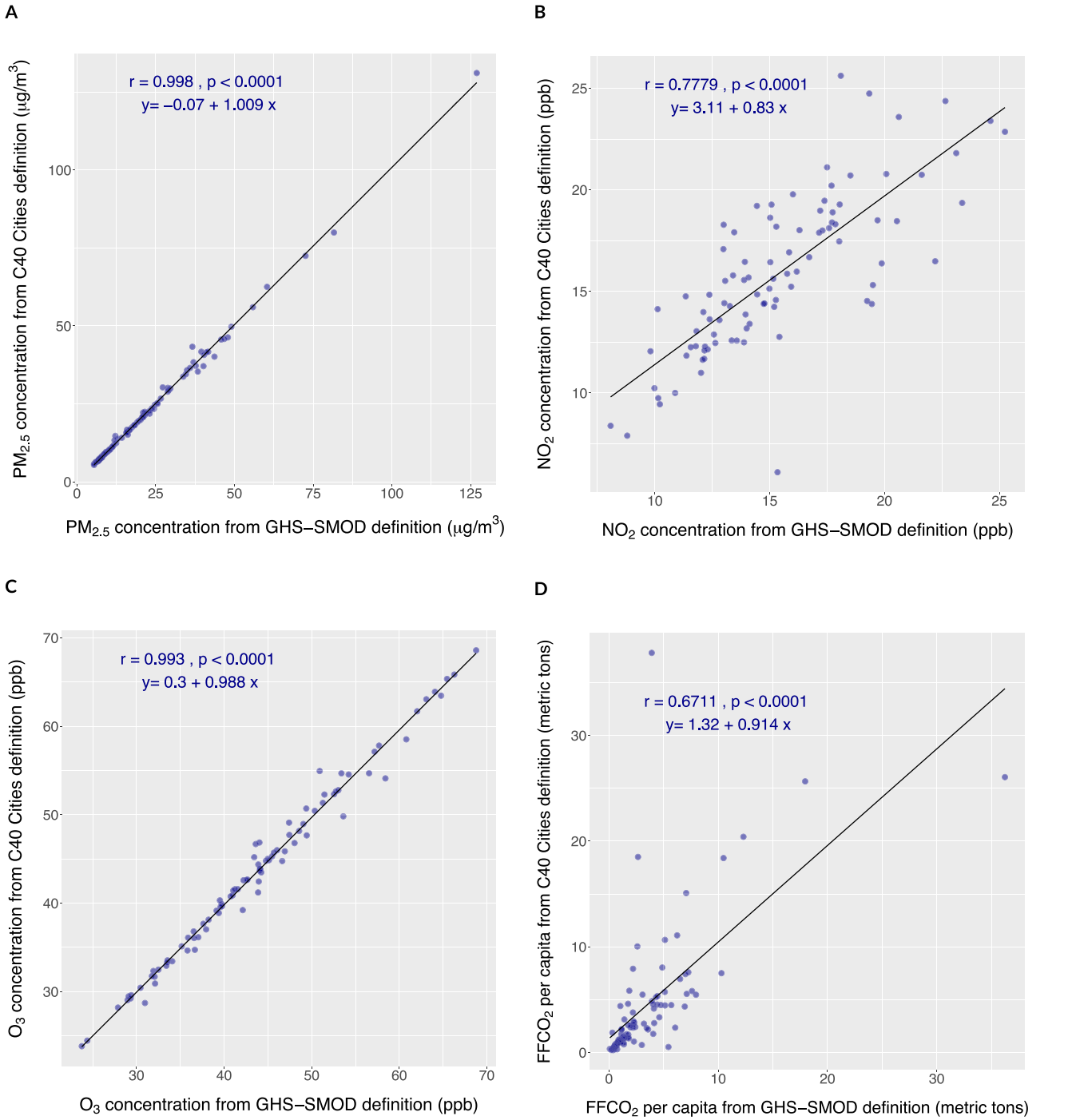


**Fig. 5 | Scatter plots of population-weighted annual average $PM_{2.5}$, $NO_2$, and OSDMA8 ($O_3$) concentrations, and $FFCO_2$ per capita in 2019 derived from two different urban boundary definitions.** **A** Population-weighted annual average $PM_{2.5}$ (μg/m$^3$); $n = 92$. **B** Population-weighted annual average $NO_2$ (ppb); $n = 92$. **C** Population-weighted OSDMA8 ($O_3$) (ppb); $n = 90$. **D** $FFCO_2$ per capita (metric tons); $n = 92$.

trends, we calculated the mean of population-weighted annual averages of all urban areas across the globe or a specific GBD super-region (i.e., an average of averages), while Anenberg et al. calculated the population-weighted average of all urban grid cells across each region at once[20]. These differences between studies may collectively lead to different final estimates of urban $NO_2$. However, we expect that the new $NO_2$ estimates from Larkin et al. might provide better estimates as this dataset has a higher prediction performance with an $R^2$ of 0.63 globally, compared to 0.54 in Anenberg et al.[20,32], which is likely due to the use of a larger set of predictor variables, finer spatial resolution in the input data, and a greater volume of training data.

We found positive correlations between long-term trends of the four pollutants across the majority of urban areas worldwide. Specifically, we found more conclusive evidence of a correlation between urban $PM_{2.5}$ and $O_3$ concentrations across different analyses. These findings provide empirical evidence on the co-emission patterns of these four pollutants and/or their precursors, further stressing the co-benefits of air pollution and climate actions in reducing both air pollutants and $CO_2$ emissions. Some literature has reported positive correlations between long-term trends of $PM_{2.5}$ and $NO_2$ concentrations, primarily driven by the contribution of traffic emissions[33–35]. We found stronger evidence of a positive correlation between annual $PM_{2.5}$ and $O_3$ levels, but the available evidence on the

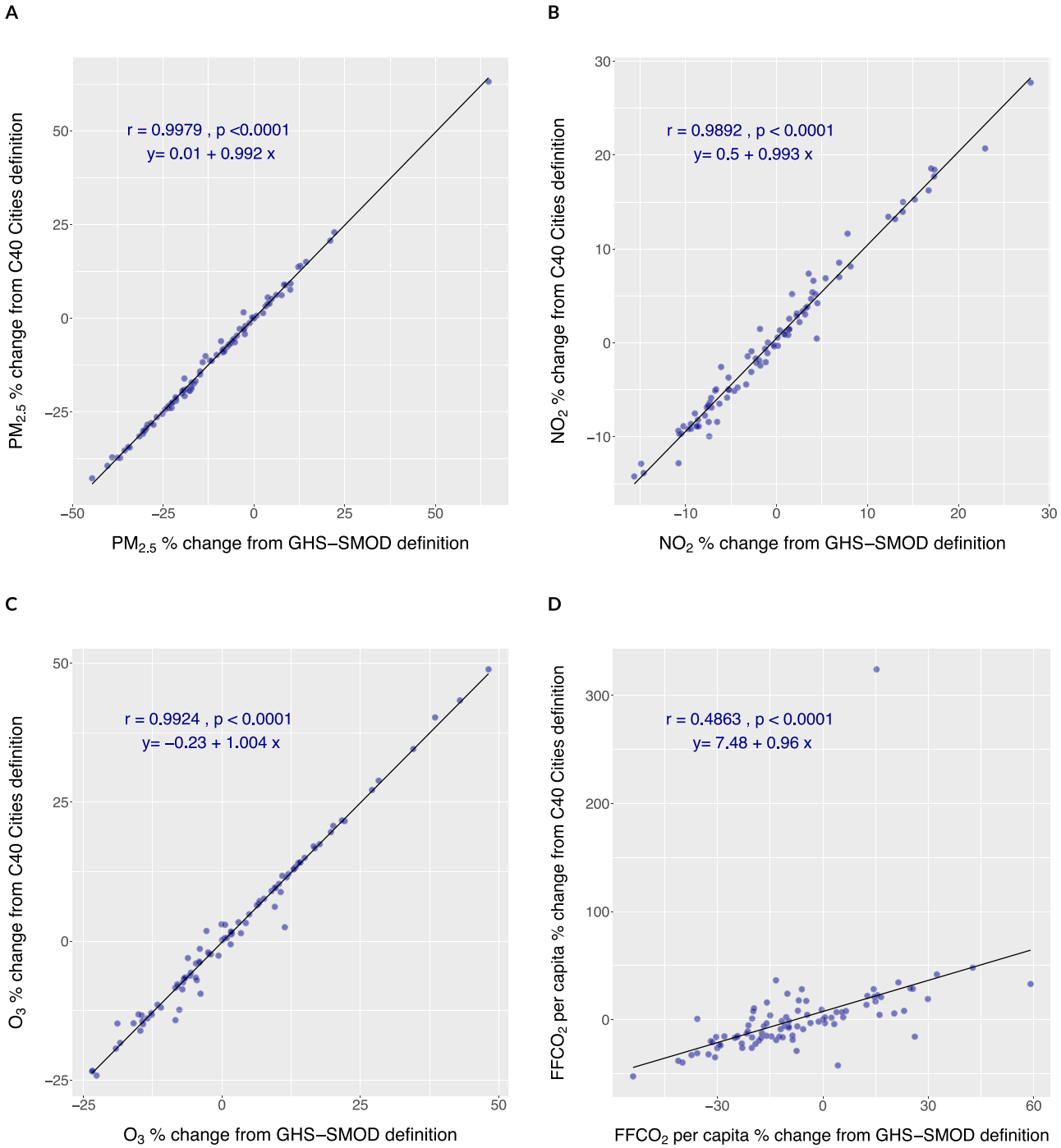


**Fig. 6 | Scatter plots of percent changes of population-weighted annual average $PM_{2.5}$, $NO_2$, and OSDMA8 ($O_3$) concentrations, and $FFCO_2$ per capita from 2005–2007 to 2017–2019, derived from two different urban boundary definitions.** **A** Population-weighted annual average $PM_{2.5}$ (μg/m$^3$); $n = 92$. **B** Population-weighted annual average $NO_2$ (ppb); $n = 92$. **C** Population-weighted OSDMA8 ($O_3$) (ppb); $n = 90$. **D** $FFCO_2$ per capita (metric tons); $n = 92$.

correlations of long-term averaged $O_3$ concentrations with the other two air pollutants is mixed and limited[35–39]. Studies reporting positive correlations between $O_3$ and the other two pollutants suggest that this may be because $O_3$ precursors, such as nitrogen oxides ($NO_x$) and volatile organic compounds (VOCs), are closely related to the formation of secondary $PM_{2.5}$ and $NO_2$[35,40]. Specifically for $PM_{2.5}$, some studies have reported that its correlation with $O_3$ may arise from their dependency on specific meteorological factors such as temperature inversion and atmospheric stagnation since both pollutants are secondary pollutants (partially for $PM_{2.5}$)[38,39]. However, due to the intricate chemical reactions of $O_3$, the evidence remains inconsistent across different spatiotemporal contexts, making it challenging to get a globally unified interpretation of its correlations with other pollutants. Regarding $CO_2$ emissions, only a few studies have investigated its relationship with $PM_{2.5}$ concentration using observational data[41,42]. Many studies have identified its potential correlations with air pollution only indirectly, inferring from air quality models assuming their co-emissions from common sources[26,43,44].

Given the common emission sources among the pollutants and/or their precursors, we hypothesized that we might uncover consistently positive correlations among these pollutant trends. Although we found that positive correlations dominate in many cases, positive correlations were not always dominant, particularly in urban areas in Latin America and

Caribbean and North Africa and Middle East (Fig. 4). Long-term trends of air pollution are not exclusively influenced by local emissions, but also by various factors like meteorological conditions, natural emissions, and long-range transport, with variations arising from the distinct formation characteristics of different pollutants. For example, reducing NOx emissions may decrease $NO_2$ and $PM_{2.5}$ concentrations but could leave $O_3$ levels unchanged or even increased due to complexities in $O_3$-NOx-VOC chemistry[45]. Climate change and rising temperature also affect air pollutant emissions from natural sources, such as increased wildfire activities[46], which release air pollutants independently of anthropogenic emissions, unlike $FFCO_2$. The impacts of climate change can vary across air pollutants; for instance, natural sources of $O_3$ precursors include biogenic VOCs, soil NOx, wetland methane, and wildfires[47], whereas $PM_{2.5}$ is more heavily impacted by wildfires and natural dust[48]. Additionally, the fact that $O_3$ formation accelerates at higher temperatures[49], along with increased emissions of its precursors from natural sources, could explain why $O_3$ concentrations showed significant increases globally across all four pollutants. Lastly, pollutants like $PM_{2.5}$ and $O_3$ can be transported across regions and even hemispheres by large-scale air circulation, as $O_3$ has a relatively long atmospheric lifetime and both pollutants have long-lived precursors[47,50,51]. As a result, long-range transport can either offset or amplify the impacts of local emission changes in certain areas.

While the pollutants considered in our study and/or their precursors are co-emitted, long-term trends of air pollutants and $CO_2$ emissions can be independently influenced by different emission reduction strategies or exogenous events (e.g., armed conflicts and migration)[22,52,53]. For example, while renewable and nuclear energy can effectively mitigate both air pollutants and $FFCO_2$ emissions, carbon capture and storage have no impacts on improving air quality but effectively mitigate $FFCO_2$ emissions, and motor vehicle tailpipe controls can only mitigate air pollution[22]. Therefore, further studies are needed to explain how different combinations of mitigation strategies and regional events influence long-term trends of each pollutant, particularly in areas showing opposing and decoupling trends among pollutants like Latin America and Caribbean and in North Africa and Middle East.

The variations in trends and correlation patterns we found across GBD super-regions likely stem from differences in primary sources of pollutants and regional environmental and socioeconomic contexts. For instance, urban areas in High-income countries showed significant decreases in all four pollutants and positive correlations between pollutant trends. These findings may reflect the impacts of comprehensive air pollution control strategies, active support mechanisms for reducing GHGs emissions, and their synergistic impacts in High-income countries, including many Western European, North American, and East Asian countries. For example, the US has regulated criteria air pollutants under the Clean Air Act and has strengthened the regulations continuously over time, incorporating various strategies like establishing emission standards for primary emission sources. Additionally, federal- and state-level GHGs mitigation actions, including renewable portfolio standards, increased investment in research and development, and renewable energy tax credits, have supported the transition to renewable energy in the energy sector[54–56]. This transition, coupled with a simultaneous increase in natural gas use, replacing coal[57], has resulted in reductions of both total emissions and per capita emissions of $FFCO_2$[58]. Also, as several measures overlap between air pollution and climate actions, such as increasing the use of renewable energy and cleaner fuels and increasing motor vehicle fuel efficiency, these overlapping measures might contribute to complementary reductions of both air pollution and $CO_2$ emissions[22,59].

On the other hand, urban areas in South Asia and Sub-Saharan Africa experienced large increases in air pollution and/or $FFCO_2$ per capita, resulting in largely positive correlations in their temporal trends. Such trends might be attributable to rapid economic growth in these regions as these two regions experienced among the largest economic and population growths, leading to large increases in fossil fuel use in transportation, industrial sources, and power plants sectors[60–62]. While South Asian countries have begun controlling emissions of air pollutants and GHGs during the study period by setting emission standards and transitioning to cleaner energy, especially focusing on vehicle emissions, the influence of these actions was likely outweighed by rapid urbanization and economic growth[63,64]. Some studies have suggested that the lack of public awareness, appropriate air quality monitoring, political support, and international cooperation could also lead to the ineffectiveness of the control measures in these regions[63,65]. In Sub-Saharan Africa, as urbanization is still in its early stages and household air pollution has been a major focus in policies, there has been less action addressing ambient air pollution, likely combined with a lack of political will and capacity[62,66]. As a result, the region might have been unable to effectively counter the increasing emissions from economic growth and urbanization. Some studies have suggested various policy options for countries in these regions, which decouple air pollution and GHGs emissions from economic growth while not impeding growth itself, including improved energy efficiency, public transport, waste management, and increased use of cleaner cook stoves[64,67]. By adopting these strategies, these regions might effectively achieve both developmental and environmental goals simultaneously.

We compared two urban boundary definitions–from GHS-SMOD and C40 Cities–both of which have important roles in research and policy. The GHS-SMOD is one of the most frequently used urban boundary datasets in scientific research that provides a globally consistent characterization of urban areas. On the other hand, the urban boundary datasets from the C40 Cities may better reflect the scale at which city-level policies are implemented. We found that the different urban definitions influenced urban $NO_2$ concentrations and $FFCO_2$ per capita in 2019, while $PM_{2.5}$ and $O_3$ concentrations were largely insensitive to urban definitions. However, the agreement was still at moderate to high levels with correlation coefficients over 0.6. Several studies have reported variations in urban estimates of air pollution and $CO_2$ emissions by different urban definitions[68–71]. Discrepancies in $NO_2$ estimates from different urban definitions likely reflect its high intraurban spatial heterogeneity due to localized pollution hotspots and short lifetime[72,73]. Similarly, $FFCO_2$ per capita can vary with urban definitions, as emission estimates are directly derived from the geographic distribution of emission sources, which may differ between city centers and suburbs–for instance, suburbs often have more large point sources than city centers[71,74]. Also, certain sources may emit different amounts of $CO_2$ emissions between urban centers and suburbs, which can make urban $CO_2$ emission estimates sensitive to urban boundary definitions. For example, several studies found that people living in suburbs are more likely to have higher commuting $CO_2$ emissions than city centers due to longer-distance commuting travel[74,75]. Therefore, in future studies, particularly those focused on $NO_2$ concentrations and $CO_2$ emissions, researchers should use urban definitions that are appropriate for their research objectives and exercise caution when comparing findings with other studies that might have relied on other urban definitions.

This study has some limitations. First, while this study utilized recent-developed global datasets of air pollution and GHGs incorporating state-of-the-art methods to improve the accuracy of measurements, these datasets may still contain errors due to insufficient input data, incorrect model processes, and erroneous emission data[20,76–78]. Second, the level of prediction errors in the air pollutant datasets can differ by global regions. Global estimates of $PM_{2.5}$, $NO_2$, and $O_3$ concentrations incorporate to varying degrees ground-level monitors that are predominantly located in High-income countries within the Global North, and estimated concentrations are likely more uncertain for unmonitored urban areas in the Global South. Van Donkelaar et al. and DeLang et al. reported the largest uncertainty estimates of global $PM_{2.5}$ and $O_3$ concentrations, respectively, in under-monitored regions, as shown in Supplementary Table 4[76,77]. Accordingly, we observed the lowest absolute uncertainties in High-income countries when compared to the other regions for both $PM_{2.5}$ and $O_3$ (Supplementary Table 4). We expect that using satellite data with complete global coverage used as inputs in these datasets might ameliorate this potential for $PM_{2.5}$ and $NO_2$. However, direct satellite observations are unavailable for $O_3$ due to the

high abundance of $O_3$ in the upper atmosphere, making $O_3$ estimates in regions without monitoring stations and $O_3$ distributions at the fine spatial scale rely primarily on bias-corrected models rather than direct observations. Third, additional uncertainty may also arise from the population dataset due to the absence of consistently available sub-national census datasets at fine scales and the inaccuracy in those source datasets[79,80].

Fourth, our results may be influenced by the choice of spatial resolution in the prediction models. In our study, $O_3$ and $CO_2$ datasets have a coarser resolution of 10 km, compared to $PM_{2.5}$ (1 km) and $NO_2$ (50 m). Several studies found that coarse model resolutions that fail to capture smaller-scale variations in air pollutant concentrations can underestimate pollution levels due to the smoothing of hotspots[81–84]. Also, many urban areas are represented by only a single or a few grid cells for $O_3$ concentration and $FFCO_2$ per capita (92% of urban areas have total areas smaller than 100 $km^2$). While some studies found no significant improvement in accuracy with resolutions finer than 10 km for $O_3$, given its nature as a secondary pollutant with less spatial variation[85,86], $CO_2$ emissions can vary substantially at small scales due to its dependence on specific locations of emission sources. For $PM_{2.5}$ and $NO_2$, although, to the best of our knowledge, the datasets we used have the finest resolutions among existing global models, it still remains uncertain whether these resolutions are fine enough to capture small-scale variations. Moreover, fine model resolutions may sometimes compromise predictive power and require additional computational costs[85]. For example, the $NO_2$ dataset has lower prediction power than the other two pollutants, with $R^2$ of 0.84, 0.63, and 0.81 for $PM_{2.5}$, $NO_2$, and $O_3$, respectively. Therefore, while finer model resolutions are essential to resolve fine-scale urban gradients of the pollutants, researchers should carefully weigh the trade-offs between achieving finer resolutions and the associated computational demands and potential impacts on model performance. Lastly, the GHS-SMOD urban boundary definition we used is from 2015 estimates[87]. As urban areas have been expanding rapidly, especially those in the Global South experiencing rapid urbanization, their boundaries might have changed prior to or following 2015. However, to our knowledge, the GHS-SMOD is the only dataset to provide global coverage of all urban areas using consistent input datasets and methodologies. Additionally, using temporally varying urban boundary definitions would make it difficult to distinguish the impacts of urban actions that reduce emissions and pollution from those of city expansion or diminution. Therefore, we used 2015 GHS-SMOD urban boundary definitions.

Despite these limitations, we provide one of the first systematic comparisons of global trends of $PM_{2.5}$, $NO_2$, and $O_3$ concentrations and $FFCO_2$ per capita in urban areas. Given that urban areas have been hubs of air pollutants and GHG emissions, as well as the focus of diverse mitigation actions undertaken globally, our findings highlight the outcomes of past urban initiatives and provide insights for future strategies in different global regions. By examining potential correlations between pollutant trends globally and across various regions using datasets that are based on historical observations, we provide empirical evidence on ways that air pollution and GHGs emissions are coupled and might be simultaneously mitigated. The regional variations in the results, such as the contrasting trends between High-income countries and South Asia or Sub-Saharan Africa, stress the need to further understand the local and regional drivers of air pollution and GHGs emissions and tailored region-specific strategies. Furthermore, the influence of different urban boundary definitions on pollutant estimates underscores the importance of how we define urban air pollution and $CO_2$ emissions in research and policy.

## Methods

### Population-weighted annual average $PM_{2.5}$, $NO_2$, and OSDMA8 ($O_3$) concentrations and $FFCO_2$ per capita

We leveraged existing global, highly spatially-resolved datasets of $PM_{2.5}$, $NO_2$, and $O_3$ that represent the current state-of-the-science estimates of each pollutant. Specifically, we used a global $PM_{2.5}$ dataset for 2000–2020 from van Donkelaar et al.[77], which estimates annual average concentrations at 0.01° (~1 km) resolution, combining satellite remote sensing of aerosol optical depth, a chemical transport model, and ground-based measurements. For $NO_2$, we employed a global dataset for 2005–2020 from Larkin et al. This dataset provides annual average concentrations at 50 m resolution using a land-use regression model that ingests remotely-sensed measurements from the OMI with other land use variables, trained against ground-based measurements worldwide[32]. For $O_3$, we used a global dataset for 2000–2020 from the GBD 2019 study[88], which is extrapolated from an $O_3$ dataset of Delang et al.[76]. This dataset estimated the annual maximum of the six-month running mean of the monthly average daily maximum 8 h mixing ratio (ozone season daily maximum 8 h mixing ratios, OSDMA8) at 0.1° (~10 km) resolution combining ground-based $O_3$ observations from the Tropospheric Ozone Assessment Report (TOAR) and the Chinese National Environmental Monitoring Center Network, and outputs from multiple global atmospheric models[76,88].

Evaluations of these datasets against ground-based observations revealed a high degree of agreement (i.e., $R^2$ of 0.84, 0.63, and 0.81 for $PM_{2.5}$, $NO_2$, and $O_3$, respectively) and improved predictive performance over previous global estimates of these pollutants[32,76,77]. Also, by using the annual averaged $PM_{2.5}$ and $NO_2$ concentrations and the annual maximum of the six-month running mean for $O_3$, which is likely to include mostly warm season concentrations, we effectively controlled day-to-day and seasonal variations of air pollution, and thus these estimates are likely to reflect the impacts of long-term emission changes.

To calculate $FFCO_2$ per capita, we used annual sector-specific emission datasets of the Emission Database for Global Atmospheric Research (EDGAR) v8.0 for 2000-2020, which has 0.1° (~10 km) resolution with global coverage[89]. The EDGAR dataset contains emissions of multiple GHG species, but we only considered $CO_2$ emissions emitted from anthropogenic sources within each grid cell. This dataset provides production-based $CO_2$ emissions, which account for $CO_2$ emissions in the location where goods and services are produced, rather than where they are consumed. For example, even if a certain amount of $CO_2$ is emitted from producing goods that are exported and used outside a grid cell, the emissions are still accounted for in the total $CO_2$ emission of that grid cell. We defined $FFCO_2$ emissions as a sum of total emissions from all sectors of anthropogenic sources, including power industry, industrial combustion and processes, buildings, transport, agriculture, fuel exploitation, and waste[19]. While $PM_{2.5}$, $O_3$, and $FFCO_2$ per capita are available annually from 2000 to 2020, $NO_2$ estimates are only available annually from 2005 to 2020 because OMI, which provides remotely-sensed $NO_2$ measurements used by the land-use regression model used to estimate surface-level $NO_2$, was launched in 2004.

To compute the urban estimates, we used 2015 GHS-SMOD urban boundaries for 13,189 urban areas worldwide[87]. The GHS-SMOD urban boundaries were defined by the European Commission based on global geographic distribution of populations and urban structures[87]. We additionally obtained global gridded population counts for 2000–2020 at 1 km resolution from WorldPop, which incorporates country-specific population estimates and population-related geospatial factors[90]. We regridded the air pollutant and $CO_2$ datasets to the same 1 km resolution and extent as WorldPop. For each urban area defined by the GHS-SMOD, we calculated population-weighted average of $PM_{2.5}$ (gridded annual average), $NO_2$ (gridded annual average), and $O_3$ (gridded OSDMA8) concentrations, as well as $FFCO_2$ per capita. Population-weighted average concentrations were calculated using Eq. (1):

$$c_{i,population-weighted} = \sum_j (p_{i,j} \times c_{i,j}) / \sum_j p_{i,j} \quad (1)$$

where $c$ represents pollutant concentration, $i$ denotes an urban area, $j$ denotes a grid cell in urban area $i$, and $p$ represents population count. $FFCO_2$ per capita was calculated by dividing the total $FFCO_2$ emissions in an urban area by the total population of that urban area. In the calculations, grid cells with missing values in either pollutants or population datasets were excluded. Missing grid cells were primarily located over oceans and inland water bodies. The total number of cities varies by year and pollutant due to

differences in the pollutant datasets, and details on these variations are provided in the figure captions.

### Temporal trends for 2005-2019

Urban population-weighted annual average $PM_{2.5}$, $NO_2$, and OSDMA8 ($O_3$) concentrations and $FFCO_2$ per capita were aggregated globally and across GBD super-regions for every year by calculating mean values of air pollutant concentrations and median values of $FFCO_2$ per capita overall urban areas within each region. For $FFCO_2$ per capita, because of the high variation and extreme values, we used the median as a summary statistic instead of the mean. The GBD super-region categorization groups countries into seven large regions based on geographic proximity and similarity of epidemiological patterns (Supplementary Fig. 1)[91]. While we visualize trends in pollutants from 2000 to 2020 (2005–2020 for $NO_2$) (e.g., Fig. 2), our statistical analysis of trends (e.g., Fig. 3) is based on 2005-2019 due to $NO_2$ data availability starting from 2005 and 2019 being the latest year unaffected by the COVID-19 pandemic. In the main analyses, we summarized temporal trends as percent changes in pollutant levels by comparing the 3-year average of annual means/medians from 2005 to 2007 to that from 2017–2019. Here, we used 3-year averages to minimize the influence of outliers from any single year. Additionally, the significance of monotonic temporal trends between 2005 and 2019 was tested using the Mann-Kendall test.

Then, we calculated the Pearson correlation coefficient ($r$) characterizing the temporal correlations among population-weighted annual average $PM_{2.5}$, $NO_2$, and OSDMA8 ($O_3$) concentrations and $FFCO_2$ per capita. These coefficients were calculated at the city level, which resulted in six different correlation coefficients of every possible pair of the four pollutants for every individual city, and then were summarized at GBD super-regions and globally. At the aggregated level, we present the proportions of urban areas with four categories of correlation coefficients: significant positive, non-significant positive, significant negative, and non-significant negative. Statistical significance for all statistical tests in this study was set at the 95% confidence level, where a p-value less than 0.05 was considered statistically significant.

### Urban boundary analysis

We tested the influence of two different urban boundary definitions on our estimates of the four pollutants: the GHS-SMOD definition, which was used for our primary results as this is the most frequently used definition in global-scale research[13,20,21,92,93], and the C40 Cities definition. As stated before, the GHS-SMOD urban boundaries were defined based on global geographic distribution of populations and urban structures[87]. The C40 Cities definition relies on self-reported urban boundaries from their 97 member cities, and boundaries for a particular city might include broader geographic areas (e.g., suburbs, exurbs) than just the immediate urban areas. We compared annual level estimates of the four pollutants in 2019 and temporal trends for 2005−2019 from the two different definitions, across 92 urban areas (90 urban areas for $O_3$ due to missing values in the $O_3$ dataset) represented by both GHS-SMOD and C40 Cities. For temporal trends, we used the same percent change metric as in our temporal trends analysis. Additionally, to understand how differing urban boundary definitions can influence public health implications regarding urban air pollution, we compared the numbers of cities exceeding the WHO AQGs and the population living in those cities, estimated from the two urban definitions.

To identify potential drivers of the differences in pollutant estimates between urban boundary definitions, we correlated the differences in pollutant estimates between GHS-SMOD and C40 Cities definitions with several urban characteristics. These characteristics include total area, total population, population density from the GHS-SMOD, the difference in population and area between GHS-SMOD and C40 Cities, and Moran's I. Here, Moran's $I$ characterizes the level of spatial autocorrelation of pollutant estimates within a given city included in the GHS-SMOD. We correlated the differences in pollutant levels with these metrics using Pearson and Spearman correlations depending on the distribution of the variable (Supplementary Table 3).

## Data availability

The datasets generated during the current study are available in CSV format from the author's GitHub repository (https://github.com/sooyeon-kim-29/Tracking-air-pollution-and-CO2-emissions….git) and GW Air, Climate, and Health lab's website (https://blogs.gwu.edu/sanenberg/pm2-5-no2-and-ozone-data-for-13000-cities-worldwide/) with online data visualization tools. $PM_{2.5}$ datasets used in the current study are available via the Washington University Atmospheric Composition Analysis Group website (https://sites.wustl.edu/acag/datasets/surface-pm2-5/), and $O_3$ datasets are available through our co-author's repository on Zenodo (https://zenodo.org/records/8320001).

## Code availability

The code used for the current study is available from the author's GitHub repository (https://github.com/sooyeon-kim-29/Tracking-air-pollution-and-CO2-emissions….git).

Received: 20 August 2024; Accepted: 2 April 2025;
Published online: 07 May 2025

## References

1. Raaschou-Nielsen, O. et al. Air pollution and lung cancer incidence in 17 European cohorts: prospective analyses from the European Study of Cohorts for Air Pollution Effects (ESCAPE). *Lancet Oncol.* **14**, 813–822 (2013).
2. Jacobs, M. et al. The association between ambient air pollution and selected adverse pregnancy outcomes in China: a systematic review. *Sci. Total Environ.* **579**, 1179–1192 (2017).
3. Turner, M. C. et al. Long-term ozone exposure and mortality in a large prospective study. *Am. J. Respir. Crit. Care Med.* **193**, 1134–1142 (2016).
4. Boogaard, H. et al. Long-term exposure to traffic-related air pollution and non-accidental mortality: a systematic review and meta-analysis. *Environ. Int.* **176**, 107916 (2023).
5. Rodríguez-Villamizar, L. A., Rojas-Roa, N. Y., Blanco-Becerra, L. C., Herrera-Galindo, V. M. & Fernández-Niño, J. A. Short-term effects of air pollution on respiratory and circulatory morbidity in Colombia 2011–2014: a multi-city, time-series analysis. *Int. J. Environ. Res. Public Health* **15**, 1610 (2018).
6. Brauer, M. et al. Global burden and strength of evidence for 88 risk factors in 204 countries and 811 subnational locations, 1990–2021: a systematic analysis for the Global Burden of Disease Study 2021. *Lancet* **403**, 2162–2203 (2024).
7. IPCC. IPCC, 2023: Summary for policymakers. In: *Climate Change 2023: Synthesis Report. Contribution of Working Groups I, II and III to the Sixth Assessment Report of the Intergovernmental Panel on Climate Change* [Core Writing Team, H. Lee and J. Romero (eds.)] 1–34 (IPCC, 2023)
8. Perkins-Kirkpatrick, S. E. & Lewis, S. C. Increasing trends in regional heatwaves. *Nat. Commun.* **11**, 3357 (2020).
9. UN-Habitat. *Cities and Climate Change: Global Report on Human Settlements* (Routledge, 2011).
10. Larkin, A., van Donkelaar, A., Geddes, J. A., Martin, R. V. & Hystad, P. Relationships between changes in urban characteristics and air quality in East Asia from 2000 to 2010. *Environ. Sci. Technol.* **50**, 9142–9149 (2016).
11. Hoek, G. et al. A review of land-use regression models to assess spatial variation of outdoor air pollution. *Atmos. Environ.* **42**, 7561–7578 (2008).
12. Bongaarts, J. United nations department of economic and social affairs, population division world mortality report 2005. *Popul. Dev. Rev.* **32**, 594–596 (2006).

13. Malashock, D. A. et al. Global trends in ozone concentration and attributable mortality for urban, peri-urban, and rural areas between 2000 and 2019: a modelling study. *Lancet Planet Health* **6**, e958–e967 (2022).
14. Strosnider, H., Kennedy, C., Monti, M. & Yip, F. Rural and urban differences in air quality, 2008–2012, and community drinking water quality, 2010–2015—United States. *MMWR Surveill. Summ.* **66**, 1 (2017).
15. UN. Transforming our world: the 2030 Agenda for Sustainable Development. UN Doc A/RES/70/1. United Nations General Assembly; [cited 7 Jul 2024]. Available from: https://www.un.org/en/development/desa/population/migration/generalassembly/docs/globalcompact/A_RES_70_1_E.pdf (2015).
16. C40 Cities. CLEAN AIR ACCELERATOR: How cities are cleaning the air we breathe. C40 Cities;[cited 7 Jul 2024]. Available from: https://www.c40.org/wp-content/uploads/2024/03/C40_Clean_Air_Accelerator_Progress_Report_2023.pdf (2023).
17. Castells-Quintana, D., Dienesch, E. & Krause, M. Air pollution in an urban world: a global view on density, cities and emissions. *Ecol. Econ.* **189**, 107153 (2021).
18. Sicard, P. et al. Trends in urban air pollution over the last two decades: a global perspective. *Sci. Total Environ.* **858**, 160064 (2023).
19. Crippa, M. et al. GHG emissions of all world countries. Publications Office of the European Union https://publications.jrc.ec.europa.eu/repository/handle/JRC126363 (2021).
20. Anenberg, S. C. et al. Long-term trends in urban NO2 concentrations and associated paediatric asthma incidence: estimates from global datasets. *Lancet Planet Health* **6**, e49–e58 (2022).
21. Southerland, V. A. et al. Global urban temporal trends in fine particulate matter (PM2· 5) and attributable health burdens: estimates from global datasets. *Lancet Planet Health* **6**, e139–e146 (2022).
22. West, J. J. et al. Air quality. In: Crimmins A. R., Avery C. W., Easterling D. R., Kunkel K. E., Stewart B. C., Maycock T. K., editors. *Fifth National Climate Assessment* (U.S. Global Change Research Program, 2023).
23. McClure, C. D. & Jaffe, D. A. US particulate matter air quality improves except in wildfire-prone areas. *Proc. Natl. Acad. Sci.* **115**, 7901–7906 (2018).
24. Xie, Y. et al. Co-benefits of climate mitigation on air quality and human health in Asian countries. *Environ. Int* **119**, 309–318 (2018).
25. Anenberg, S. C. et al. Global air quality and health co-benefits of mitigating near-term climate change through methane and black carbon emission controls. *Environ. Health Perspect.* **120**, 831–839 (2012).
26. West, J. J. et al. Co-benefits of mitigating global greenhouse gas emissions for future air quality and human health. *Nat. Clim. Chang.* **3**, 885–889 (2013).
27. Zhou, Q., Nizamani, M. M., Zhang, H. Y. & Zhang, H. L. The air we breathe: An In-depth analysis of PM2. 5 pollution in 1312 cities from 2000 to 2020. *Environ. Sci. Pollut. Res.* **30**, 93900–93915 (2023).
28. Parker, S. & Bhatti, M. I. Dynamics and drivers of per capita CO2 emissions in Asia. *Energy Econ.* **89**, 104798 (2020).
29. Muntean, M. et al. Fossil $CO_2$ Emissions of All World Countries. Vol. 2 (Publications Office of the European Union, 2018).
30. Dong, F., Wang, Y., Su, B., Hua, Y. & Zhang, Y. The process of peak CO2 emissions in developed economies: a perspective of industrialization and urbanization. *Resour. Conserv Recycl.* **141**, 61–75 (2019).
31. IEA, World Energy Statistics and Balances, IEA, Paris [cited 7 Jul 2024]. Available from: https://www.iea.org/data-and-statistics/data-product/world-energy-statistics-and-balances (2024).
32. Larkin, A. et al. A global spatial-temporal land use regression model for nitrogen dioxide air pollution. *Front. Environ. Sci.* **11**, 1125979 (2023).
33. Eeftens, M. et al. Spatial variation of PM2. 5, PM10, PM2. 5 absorbance and PMcoarse concentrations between and within 20 European study areas and the relationship with $NO_2$–results of the ESCAPE project. *Atmos. Environ.* **62**, 303–317 (2012).
34. Hazenkamp-von Arx, M. E. et al. PM2. 5 and NO2 assessment in 21 European study centres of ECRHS II: annual means and seasonal differences. *Atmos. Environ.* **38**, 1943–1953 (2004).
35. Mi, K., Zhuang, R., Zhang, Z., Gao, J. & Pei, Q. Spatiotemporal characteristics of PM2. 5 and its associated gas pollutants, a case in China. *Sustain Cities Soc.* **45**, 287–295 (2019).
36. Butenhoff, C. L. et al. Evaluation of ozone, nitrogen dioxide, and carbon monoxide at nine sites in Saudi Arabia during 2007. *J. Air Waste Manag. Assoc.* **65**, 871–886 (2015).
37. Clapp, L. J. Jenkin ME. Analysis of the relationship between ambient levels of $O_3$, $NO_2$ and NO as a function of NOx in the UK. *Atmos. Environ.* **35**, 6391–6405 (2001).
38. Kerr, G. H. & Waugh, D. W. Connections between summer air pollution and stagnation. *Environ. Res. Lett.* **13**, 084001 (2018).
39. Shao, M. et al. Co-occurrence of surface O3, PM2. 5 pollution, and tropical cyclones in China. *J. Geophys. Res. Atmos.* **127**, e2021JD036310 (2022).
40. Liao, K. J. et al. Current and future linked responses of ozone and PM2. 5 to emission controls. *ACS Publ.* **42**, 4670–4675 (2008).
41. Li, Y. et al. Spatial characteristics of CO2 emissions and PM2. 5 concentrations in China based on gridded data. *Appl. Energy* **266**, 114852 (2020).
42. Anenberg, S. C. et al. Particulate matter-attributable mortality and relationships with carbon dioxide in 250 urban areas worldwide. *Sci. Rep.* **9**, 11552 (2019).
43. Driscoll, C. T. et al. US power plant carbon standards and clean air and health co-benefits. *Nat. Clim. Chang.* **5**, 535–540 (2015).
44. Zhang, Y., Smith, S. J., Bowden, J. H., Adelman, Z. & West, J. J. Co-benefits of global, domestic, and sectoral greenhouse gas mitigation for US air quality and human health in 2050. *Environ. Res. Lett.* **12**, 114033 (2017).
45. Liu, C. & Shi, K. A review on methodology in O3-NOx-VOC sensitivity study. *Environ. Pollut.* **291**, 118249 (2021).
46. Kinney, P. L. Climate change, air quality, and human health. *Am. J. Prev. Med.* **35**, 459–467 (2008).
47. Dewan, S. & Lakhani, A. Tropospheric ozone and its natural precursors impacted by climatic changes in emission and dynamics. *Front. Environ. Sci.* **10**, 1007942 (2022).
48. McDuffie, E. E. et al. Source sector and fuel contributions to ambient PM2. 5 and attributable mortality across multiple spatial scales. *Nat. Commun.* **12**, 1–12 (2021).
49. Bloomer, B. J., Stehr, J. W., Piety, C. A., Salawitch, R. J. & Dickerson R. R. Observed relationships of ozone air pollution with temperature and emissions. *Geophys. Res. Lett*. **36**, L09803 (2009).
50. Moran, M. D., Dastoor, A. & Morneau, G. Long-range transport of air pollutants. In *Air Quality Management: Canadian Perspectives on a Global Issue* (eds Taylor, E. & McMillan, A.). 69–98 (Springer, New York, 2013).
51. Chen, T. F., Chang, K. H. & Tsai, C. Y. Modeling direct and indirect effect of long range transport on atmospheric PM2. 5 levels. *Atmos. Environ.* **89**, 1–9 (2014).
52. Zalakeviciute, R. et al. War impact on air quality in Ukraine. *Sustainability* **14**, 13832 (2022).
53. Kouyakhi, N. R. CO2 emissions in the Middle East: decoupling and decomposition analysis of carbon emissions, and projection of its future trajectory. *Sci. Total Environ.* **845**, 157182 (2022).
54. Martinot E., Wiser R., Hamrin J. *Renewable Energy Policies and Markets in the United States* (Center for Resource Solutions, 2005)
55. Cole, W., Gates, N. & Mai, T. Exploring the cost implications of increased renewable energy for the US power system. *Electr. J.* **34**, 106957 (2021).
56. Bird, L. et al. Policies and market factors driving wind power development in the United States. *Energy Policy* **33**, 1397–1407 (2005).

57. Feng, K., Davis, S. J., Sun, L. & Hubacek, K. Drivers of the US CO2 emissions 1997–2013. *Nat. Commun.* **6**, 7714 (2015).
58. Jaforullah, M. & King, A. Does the use of renewable energy sources mitigate CO2 emissions? A reassessment of the US evidence. *Energy Econ.* **49**, 711–717 (2015).
59. Vasilakos, P. N. et al. US clean energy futures—air quality benefits of zero carbon energy policies. *Atmosphere*. **13**, 1401 (2022).
60. Kurokawa, J. & Ohara, T. Long-term historical trends in air pollutant emissions in Asia: Regional Emission inventory in ASia (REAS) version 3. *Atmos. Chem. Phys.* **20**, 12761–12793 (2020).
61. Lei, R., Feng, S. & Lauvaux, T. Country-scale trends in air pollution and fossil fuel CO2 emissions during 2001–2018: confronting the roles of national policies and economic growth. *Environ. Res. Lett.* **16**, 014006 (2020).
62. Amegah, A. K. & Agyei-Mensah, S. Urban air pollution in Sub-Saharan Africa: time for action. *Environ. Pollut.* **220**, 738–743 (2017).
63. Abdul Jabbar, S. et al. Air quality, pollution and sustainability trends in South Asia: a population-based study. *Int. J. Environ. Res. Public Health* **19**, 7534 (2022).
64. Purohit, P. et al. *Pathways to Achieve National Ambient Air Quality Standards (NAAQS) in India* (IIASA, 2019).
65. Ahmed, K., Rehman, M. U. & Ozturk, I. What drives carbon dioxide emissions in the long-run? Evidence from selected South Asian Countries. *Renew. Sustain. Energy Rev.* **70**, 1142–1153 (2017).
66. Okello, G. et al. Air quality management strategies in Africa: a scoping review of the content, context, co-benefits and unintended consequences. *Environ. Int.* **171**, 107709 (2023).
67. Wright, C. et al. Integrated Assessment of Air Pollution and Climate Change for Sustainable Development in Africa-Summary for Decision Makers. Integrated Assessment of Air Pollution and Climate Change for Sustainable Development in Africa-Summary for Decision Makers (2022).
68. Raciti, S. M., Hutyra, L. R., Rao, P. & Finzi, A. C. Inconsistent definitions of "urban" result in different conclusions about the size of urban carbon and nitrogen stocks. *Ecol. Appl.* **22**, 1015–1035 (2012).
69. Tenailleau, Q. M., Mauny, F., Joly, D., François, S. & Bernard, N. Air pollution in moderately polluted urban areas: how does the definition of "neighborhood" impact exposure assessment? *Environ. Pollut.* **206**, 437–448 (2015).
70. Cai, B. & Zhang, L. Urban $CO_2$ emissions in China: spatial boundary and performance comparison. *Energy Policy* **66**, 557–567 (2014).
71. Parshall, L. et al. Modeling energy consumption and CO2 emissions at the urban scale: Methodological challenges and insights from the United States. *Energy Policy* **38**, 4765–4782 (2010).
72. Vardoulakis, S., Solazzo, E. & Lumbreras, J. Intra-urban and street scale variability of BTEX, $NO_2$ and $O_3$ in Birmingham, UK: implications for exposure assessment. *Atmos. Environ.* **45**, 5069–5078 (2011).
73. Rodriguez-Villamizar, L. A. et al. Intra-urban variability of long-term exposure to $PM_{2.5}$ and $NO_2$ in five cities in Colombia (2023).
74. Glaeser, E. L. & Kahn, M. E. The greenness of cities: carbon dioxide emissions and urban development. *J. Urban Econ.* **67**, 404–418 (2010).
75. Liu, Y. Y., Wang, Y. Q., An, R. & Li, C. The spatial distribution of commuting CO2 emissions and the influential factors: a case study in Xi'an, China. *Adv. Clim. Change Res.* **6**, 46–55 (2015).
76. DeLang, M. N. et al. Mapping yearly fine-resolution global surface ozone through the Bayesian maximum entropy data fusion of observations and model output for 1990–2017. *Environ. Sci. Technol.* **55**, 4389–4398 (2021).
77. Van Donkelaar, A. et al. Monthly global estimates of fine particulate matter and their uncertainty. *Environ. Sci. Technol.* **55**, 15287–15300 (2021).
78. Solazzo, E. et al. Uncertainties in the Emissions Database for Global Atmospheric Research (EDGAR) emission inventory of greenhouse gases. *Atmos. Chem. Phys.* **21**, 5655–5683 (2021).
79. Kuffer, M., Owusu, M., Oliveira, L., Sliuzas, R. & van Rijn, F. The missing millions in maps: exploring causes of uncertainties in global gridded population datasets. *ISPRS Int. J. Geoinf.* **11**, 403 (2022).
80. Thomson, D. R., Leasure, D. R., Bird, T., Tzavidis, N. & Tatem, A. J. How accurate are WorldPop-Global-Unconstrained gridded population data at the cell-level? A simulation analysis in urban Namibia. *PLoS One* **17**, e0271504 (2022).
81. Valin, L. C., Russell, A. R., Hudman, R. C. & Cohen, R. C. Effects of model resolution on the interpretation of satellite $NO_2$ observations. *Atmos. Chem. Phys.* **11**, 11647–11655 (2011).
82. Cooper, M. J., Martin, R. V., McLinden, C. A. & Brook, J. R. Inferring ground-level nitrogen dioxide concentrations at fine spatial resolution applied to the TROPOMI satellite instrument. *Environ. Res. Lett.* **15**, 104013 (2020).
83. Paolella, D. A. et al. Effect of model spatial resolution on estimates of fine particulate matter exposure and exposure disparities in the United States. *Environ. Sci. Technol. Lett.* **5**, 436–441 (2018).
84. Kerr, G. H. et al. Ethnoracial disparities in nitrogen dioxide pollution in the United States: comparing data sets from satellites, models, and monitors. *Environ. Sci. Technol.* **57**, 19532–19544 (2023).
85. Sharma, S., Sharma, P. & Khare, M. Photo-chemical transport modelling of tropospheric ozone: a review. *Atmos. Environ.* **159**, 34–54 (2017).
86. Cohan, D. S., Hu, Y. & Russell, A. G. Dependence of ozone sensitivity analysis on grid resolution. *Atmos. Environ.* **40**, 126–135 (2006).
87. Pesaresi M., Florczyk A., Schiavina M., Melchiorri M., Maffenini L. GHS settlement grid, updated and refined REGIO model 2014 in application to GHS-BUILT R2018A and GHS-POP R2019A, multitemporal (1975-1990-2000-2015), R2019A. European Commission, Joint Research Centre (JRC). 10 (2019).
88. Global Burden of Disease Collaborative Network. Global Burden of Disease Study 2019 (GBD 2019) Air Pollution Exposure Estimates 1990-2019. Institute for Health Metrics and Evaluation (IHME): Seattle, United States of America; [cited 7 Jul 2024]. Available from: https://doi.org/10.6069/70JS-NC54 (2021).
89. IEA. EDGAR (Emissions Database for Global Atmospheric Research) Community GHG Database v8.0. 2023 [cited 7 Jul 2024]. Available from: https://edgar.jrc.ec.europa.eu/report_2023 (2023).
90. Tatem, A. J. WorldPop, open data for spatial demography. *Sci. Data* **4**, 1–4 (2017).
91. Murray, C. J. L. et al. GBD 2010: design, definitions, and metrics. *Lancet* **380**, 2063–2066 (2012).
92. Tuholske, C. et al. Global urban population exposure to extreme heat. *Proc. Natl. Acad. Sci.* **118**, e2024792118 (2021).
93. Zhou, Q., Liao, Y. & Wang, J. Mapping global urban greenspace: An analysis based on open land-cover data. *Urban Urban Green.* **74**, 127638 (2022).
94. The George Washington University High-performance computing cluster. Building a shared resource HPC center across university schools and institutes: a case study. arXiv:2003.13629. 30 Mar 2020. Available from: https://arxiv.org/abs/2003.13629/ (2020).


## Acknowledgements

We thank all the data providers for making their data publicly available. We thank Dan Goldberg, Arash Mohegh, Marissa N. DeLang, Michael Brauer, Perry Hystad, Andrew Larkin, Doyeon Ahn, and Sara Runkel for their role in developing and maintaining the pollutant datasets and making them publicly available. We appreciate helpful discussions from Veronica Sourtherland and Danny Malashock. We gratefully acknowledge the computing resources provided on the High-Performance Computing Cluster operated by Research Technology Services at George Washington University[94]. S.-Y. Kim, G.H. Kerr, and S.C. Anenberg acknowledge support from NASA Grants #80NSSC21K0511 and #80NSSC24K1601. R.V. Martin acknowledges support from NASA Grant #80NSSC21K0508.

## Author contributions

S.-Y. Kim: Conceptualization, Writing–original draft, Investigation & Formal analysis. G.H. Kerr: Conceptualization, Writing–review & editing & Supervision. A. van Donkelaar, R.V. Martin & J.J. West: Resources & Writing–review & editing. S.C. Anenberg: Conceptualization, Writing–review & editing, Supervision, Project administration & Funding acquisition.

## Competing interests

The authors declare no competing interests.

## Additional information

**Supplementary information** The online version contains supplementary material available at https://doi.org/10.1038/s43247-025-02270-9.

**Correspondence** and requests for materials should be addressed to Susan C. Anenberg.

**Peer review information** *Communications Earth & Environment* thanks Stefan Reis, Forrest Lacey, and the other, anonymous, reviewer(s) for their contribution to the peer review of this work. Primary Handling Editors: C. Kendra Gotangco Gonzales and Alice Drinkwater. A peer review file is available.